Fermi National Accelerator Laboratory

FERMILAB-Pub-95/121

The Stromlo-APM Redshift Survey III. Redshift Space Distortions, Omega and Bias

J. Loveday

Fermi National Accelerator Laboratory
P.O. Box 500, Batavia, Illinois 60510

G. Efstathiou

Department of Physics, Keble Road
Oxford, OX1 3RH, England

S.J. Maddox

Royal Greenwich Observatory, Madingley Road
Cambridge, CB3 0EZ, England

B.A. Peterson

Mount Stromlo and Siding Spring Observatories
Weston Creek PO, ACT 2611, Australia

May 1995

Submitted to *Astrophysical Journal*

Operated by Universities Research Association Inc. under Contract No. DE-AC02-76CHO3000 with the United States Department of Energy

Disclaimer

This report was prepared as an account of work sponsored by an agency of the United States Government. Neither the United States Government nor any agency thereof, nor any of their employees, makes any warranty, expressed or implied, or assumes any legal liability or responsibility for the accuracy, completeness, or usefulness of any information, apparatus, product, or process disclosed, or represents that its use would not infringe privately owned rights. Reference herein to any specific commercial product, process, or service by trade name, trademark, manufacturer, or otherwise, does not necessarily constitute or imply its endorsement, recommendation, or favoring by the United States Government or any agency thereof. The views and opinions of authors expressed herein do not necessarily state or reflect those of the United States Government or any agency thereof.

The Stromlo-APM Redshift Survey III. Redshift Space Distortions, Omega and Bias

J. Loveday
Fermi National Accelerator Laboratory, PO Box 500, Batavia, IL 60510, USA
loveday@fnal.gov

G. Efstathiou
Department of Physics, Keble Road, Oxford, OX1 3RH, England
gpe@oxds02.astro.ox.ac.uk

S.J. Maddox
Royal Greenwich Observatory, Madingley Road, Cambridge, CB3 0EZ, England
sjm@mail.ast.cam.ac.uk

B.A. Peterson
Mount Stromlo and Siding Spring Observatories, Weston Creek PO, ACT 2611, Australia
peterson@mso.anu.edu.au

Submitted to ApJ, 22 May 1995

Abstract

Galaxy redshift surveys provide a distorted picture of the universe due to the non-Hubble component of galaxy motions. By measuring such distortions in the linear regime one can constrain the quantity $\beta = \Omega^{0.6}/b$ where Ω is the cosmological density parameter and b is the (linear) bias factor for optically-selected galaxies. In this paper we apply two techniques for estimating β from the Stromlo-APM redshift survey — (1) measuring the anisotropy of the redshift space correlation function in spherical harmonics and (2) comparing the amplitude of the direction-averaged redshift space correlation function to the real space correlation function. We test the validity of these techniques, particularly whether the assumption of linear theory is justified, using large N-body simulations. We find that the first technique is affected by non-linearities on scales up to $\sim 30h^{-1}$Mpc. The second technique is more useful for existing redshift surveys. From the Stromlo-APM survey we find a 95% confidence upper limit of $\beta = 0.75$, with a 'best estimate' of $\beta \approx 0.48$. A bias parameter $b \approx 2$ is thus required if $\Omega \equiv 1$. However, higher-order correlations measured from the APM galaxy survey (Gaztañaga and Frieman 1994) indicate a low value for the bias parameter $b \approx 1$, requiring that $\Omega \lesssim 0.6$.

We also measure the relative bias for samples of galaxies of various luminosity and morphological type and find that low-luminosity galaxies are roughly three times less biased than L^* galaxies. For the galaxy population as a whole, we measure a real space variance of galaxy counts in $8h^{-1}$Mpc spheres of $(\sigma_8^2)_g = 0.90 \pm 0.05$.

Subject headings: galaxies: clustering — galaxies: distances and redshifts — galaxies: fundamental parameters — large-scale structure of universe — surveys

1 Introduction

Galaxy redshift surveys can provide some of the most important constraints on theories of large-scale structure, but they must be analysed with care. For pure, unperturbed Hubble flow, galaxy clustering measured in both real space and redshift space would be identical and isotropic. However, in practice, peculiar velocities will distort the redshift space correlation function. Since the amplitude of peculiar velocities depends on the cosmological density parameter Ω, by measuring this distortion we can hope to constrain the value of Ω. On small scales, the effect of peculiar velocities is to elongate clusters of galaxies along the line of sight in redshift space, leading to the well known 'fingers of God'. However, on large scales, coherent bulk flows dominate the peculiar velocity field resulting in a *compression* in the clustering pattern along the line of sight. This is illustrated for Stromlo-APM Survey galaxies in Figure 1, where we show a contour plot of the full redshift space correlation function $\xi(\sigma, \pi)$ as a function of separation parallel (π) and perpendicular (σ) to the line of sight. A compression of the low-amplitude ξ contours in the π direction compared with the σ direction is clearly visible for $\pi \gtrsim 10h^{-1}$Mpc.

This large-scale anisotropy in redshift space clustering is most naturally expressed in terms of the power spectrum. Kaiser (1987) has shown that in the linear regime of gravitational instability models, the power spectra in redshift space, $P_s(\mathbf{k})$ and real space $P_r(\mathbf{k})$ are simply related by

$$P_s(\mathbf{k}) = (1 + \beta\mu_{\mathbf{k}}^2)^2 P_r(\mathbf{k}), \tag{1}$$

where $\mu_{\mathbf{k}}$ is the cosine of the angle between the wavevector $\mathbf{k}$ and the line of sight. The amplitude of the distortion is determined by the parameter $\beta = f(\Omega)/b$, where $f(\Omega) \approx \Omega^{0.6}$ is the dimensionless growth rate of growing modes in linear theory. The bias parameter b relates the fluctuations in galaxy density to the underlying mass density in the linear regime, $\delta_g = b\delta_\rho$ for linear bias. Several practical methods for measuring β have recently been applied: measuring the anisotropy of the correlation function (Hamilton 1992, 1993a; Fisher *et al.* 1994a), the anisotropy of the power spectrum (Cole, Fisher and Weinberg 1994, 1995; Tadros *et al.* 1995) and spherical harmonics of the density field (Fisher *et al.* 1994b; Heavens and Taylor 1994).

We follow the correlation function approach in this paper.[1] Hamilton (1992) has pointed out that the cosine $\mu_{\mathbf{k}}$ in Fourier space transforms to an operator in real space:

$$\xi_s(r, \mu) = [1 + \beta(\partial/\partial z)^2(\nabla^2)^{-1}]^2 \xi_r(r), \tag{2}$$

where $(\nabla^2)^{-1}$ denotes the inverse Laplacian operator and $\mu = \hat{\mathbf{r}}.\hat{\mathbf{z}}$ is the cosine angle between pair separation $\mathbf{r}$ and the line of sight $\mathbf{z}$. The redshift space correlation function $\xi_s(r, \mu)$ is conveniently expressed as a sum of spherical harmonics involving the first three even-order Legendre polynomials, (the odd-order harmonics vanish by pair-exchange symmetry)

$$\xi_s(r, \mu) = \xi_0(r)P_0(\mu) + \xi_2(r)P_2(\mu) + \xi_4(r)P_4(\mu). \tag{3}$$

Hamilton gives expressions for the $\xi_l(r)$ in terms of integrals over $\xi_r(r)$ [his equations (6)–(9)].

To solve the inverse problem, *i.e.* to go from redshift space clustering to real space clustering, Hamilton integrates the equations describing the real and redshift space correlation functions over planes normal to the vector $\mathbf{r}$ at separation r, expands in spherical harmonics and differentiates

[1] For a power spectrum analysis of the Stromlo-APM survey, see Tadros *et al.* (1995).

with respect to r. Hamilton thereby obtains an explicit expression for β and $\xi_r(r)$ in terms of the harmonics $\xi_l(r)$ of the redshift space correlation function. Further volume averaging to minimize cancellation of terms finally results in an equation for β involving the 0th and 2nd order harmonics of the redshift space correlation function:

$$\frac{1+\frac{2}{3}\beta+\frac{1}{5}\beta^2}{\frac{4}{3}\beta+\frac{4}{7}\beta^2}=\frac{\xi_0(r)-3\int_0^r\xi_0(s)(s/r)^3ds/s}{\xi_2(r)}. \tag{4}$$

One can also write a similar expression involving the 2nd and 4th order harmonics, but in practice, as we shall see later, the 4th order harmonic is too strongly affected by non-linearity to be useful.

As well as causing anisotropy in redshift space, large-scale streaming motions also produce an amplification in the direction-averaged redshift space correlation function. For fluctuations in the linear regime, the direction-averaged redshift space correlation function $\xi(s)$ and the real space correlation function $\xi(r)$ are related by (Kaiser 1987)

$$\xi(s)\approx\left(1+\frac{2}{3}\beta+\frac{1}{5}\beta^2\right)\xi(r). \tag{5}$$

The large uncertainty in the value of β hinders comparison of $\xi(s)$ with real space predictions of galaxy clustering from various models (see, for example, Loveday *et al.* 1992a). In a recent paper (Loveday *et al.* 1995, hereafter Paper 2), we estimated the real-space correlation function of optically-selected galaxies by cross-correlating galaxies in the sparse-sampled Stromlo-APM Redshift Survey with the fully-sampled, parent APM Galaxy Survey. This projected cross-correlation function is unaffected by redshift-space distortions and may be stably inverted to give the real-space correlation function $\xi(r)$. Moreover, the large number of cross-pairs enables clustering to be measured to smaller scales than using the redshift survey data alone. If both $\xi(r)$ and $\xi(s)$ can be reliably measured in the linear regime then the value of β can be constrained using equation (5).

The above expressions (1–5) assume a plane-parallel approximation for peculiar displacements. In order to approximate this ideal in our analyses, we use only those pairs of galaxies separated by less than 50 degrees on the sky. This rejects about 20% of galaxy pairs, and, as Cole *et al.* (1994) have demonstrated, will limit deviations from the plane-parallel approximation to no more than 5% bias in the estimated value of β.

Throughout the paper, we use r to denote real space separations and s to denote separations in redshift space. Error bars on measurements from survey data are estimated using the bootstrap resampling technique (Barrow, Bhavsar and Sonoda 1984) with nine bootstrap resamplings of the survey. Error bars for simulations are determined from the variance between ten independent realizations.

The layout of the paper is as follows. The Stromlo-APM survey data and the N-body simulations are described and compared in §2. In §3 we test the estimators for β using the simulations and in §4 apply the estimators to the Stromlo-APM data. The relative bias and redshift space distortions for different galaxy types are also presented in this section. Finally, our conclusions are given in §5.

2 Comparison of Data with N-Body Simulations

Both equations (4) and (5) assume that linear theory is valid on scales on which ξ can be reliably measured. It is important to test this assumption of linearity before using these equations to estimate β. We do this by analyzing an ensemble of CDM-like N-body simulations. In this section we describe the Stromlo-APM survey data and the simulations, and show that the simulations are a realistic approximation to the data.

2.1 Stromlo-APM Survey Data

The Stromlo-APM redshift survey consists of 1787 galaxies with $b_J \leq 17.15$ selected randomly at a rate of 1 in 20 from the APM (Automated Plate Measuring) galaxy survey (Maddox *et al.* 1990a,b). The survey covers a solid angle of 1.3 sr (4300 square degrees) in the south galactic cap. The APM magnitudes have been calibrated and corrected for photographic saturation using CCD photometry as described by Loveday *et al.* 1992b (hereafter Paper 1). An approximate morphological type was assigned to each galaxy by visually inspecting the images on the United Kingdom Schmidt Telescope (UKST) survey plates. Redshifts were obtained with the Mount Stromlo-Siding Spring Observatory (MSSSO) 2.3m telescope at Siding Spring. Measured radial velocities were transformed to the local group frame using $v = v + 300\sin(l)\cos(b)$ and we assumed $\Lambda = 0$, $q_0 = 0.5$ and $H_0 = 100$ km s^{-1}Mpc^{-1} with uniform Hubble flow in calculating distances and absolute magnitudes. We adopt k-corrections for different morphological types in the b_J system as described by Efstathiou, Ellis and Peterson (1988). More details about the survey are given in Paper 1; the construction of the survey will be described in full in a future paper in this series.

2.2 Simulations

We use an ensemble of 10 N-body simulations from model B of Croft and Efstathiou (1994). These simulations combine a large volume (box length = $300h^{-1}$Mpc) with a spatial resolution of $\approx 80h^{-1}$kpc, and so can be used to generate reasonable approximations to our redshift survey. The N-body simulations have enhanced large-scale power over the standard CDM model by using a nonzero cosmological constant $\lambda = \Lambda/(3H_0^2) = (1 - \Omega_0) = 0.8$. Weights were assigned to each particle using the peak background split algorithm (Bardeen *et al.* 1986, White *et al.* 1987) and 'galaxies' selected within the APM area and with the Stromlo-APM selection function (Paper 1). This procedure produces 10 catalogues of on average 33,500 'galaxies' each. We select a subset of 1 in 20 galaxies at random from each simulated catalogue in order to mimic the sparse sampling strategy of the Stromlo-APM survey.

We measure the variance of simulated galaxy counts in $8h^{-1}$Mpc spheres in real space to be $(\sigma_8^2)_g = 1.20 \pm 0.16$. Since the simulations were evolved until the mass fluctuations $(\sigma_8^2)_m = 1.0$ (Croft and Efstathiou 1994), then the effective bias factor for 'galaxies' identified from the simulations is $b = (\sigma_8)_g/(\sigma_8)_m \approx 1.10 \pm 0.08$. A density parameter $\Omega_0 = 0.2$ was used for the simulations and hence we expect to measure $\beta \approx 0.35 \pm 0.03$ from redshift space distortions in the simulations.

2.3 Real and Redshift Space Correlation Functions

We estimate the redshift-space correlation functions from the survey and the simulations using the density-independent estimator for $\xi(s)$ discussed in Paper 2,

$$1 + \xi(s) = \frac{w_{gg}(s) w_{rr}(s)}{[w_{gr}(s)]^2}. \tag{6}$$

Here $w_{gg}(s)$, $w_{gr}(s)$ and $w_{rr}(s)$ are the summed products of weights of galaxy-galaxy, galaxy-random and random-random pairs respectively. Note that the relative densities of galaxy and random points measured at separation s are automatically accounted for by this estimator — there is no need to assume an overall galaxy density n_g. This estimator, due to Hamilton (1993b), is insensitive to variations in galaxy density and provides a very stable estimate of $\xi(s)$. For the simulations, we have the real space coordinates for each particle as well as redshift information, and so the real space correlation function $\xi(r)$ for the simulations can be calculated using the same estimator.

To calculate the real-space correlation function $\xi(r)$ for the survey data, we measure the projected cross-correlation function between the redshift data and the angular data from the fully-sampled parent catalogue,

$$\Xi(\sigma) = \int_{-\infty}^{+\infty} \xi(\sqrt{\Delta y^2 + \sigma^2}) d\Delta y, \tag{7}$$

where the integral extends over all line-of-sight separations Δy for pairs of galaxies with constant projected separation $\sigma = y\theta$ (θ is the angular separation and y is the distance to the galaxy of known redshift). This projected function is inverted numerically to give an estimate of $\xi(r)$, which is unaffected by redshift-space distortions. See Saunders *et al.* (1992) and Paper 2 for a detailed description of this estimator.

In Figure 2 we compare the clustering of galaxies in real and redshift space for the Stromlo-APM data and for the N-body simulations. For the Stromlo-APM measurements, the error bars come from the scatter between nine bootstrap resamplings of the survey (Paper 2) and for the simulations, the error bars show the scatter between ten realizations from the ensemble of simulations (Croft and Efstathiou 1994). Averaging over these realizations, $\xi(s)$ for the simulations is well fit by a power-law over 1–30 h^{-1}Mpc with parameters $\gamma_s = 1.66 \pm 0.12$ and $s_0 = 5.9 \pm 0.5$. The real-space function $\xi(r)$ has power-law parameters $\gamma_r = 2.06 \pm 0.15$ and $r_0 = 5.8 \pm 0.4$. We see that the simulations indeed match the observed clustering of galaxies reasonably well, except that the simulations tend to overestimate the clustering amplitude on non-linear scales $r \lesssim 3h^{-1}$Mpc. As discussed in Paper 2, $\xi(r)$ inferred from the cross-correlation of redshift survey galaxies with the APM data is not expected to be reliable much beyond $r \approx 20h^{-1}$Mpc, and so the 'bump' at $r \approx 30h^{-1}$Mpc should not be regarded as a serious discrepancy.

2.4 Galaxy Peculiar Velocities

If the N-body simulations are to be used to check the effects of non-linearity in the real data, then it is important to compare the amplitude of small-scale, peculiar velocities in the simulations with those in the data. By comparing estimates of clustering in redshift space and real space, one can constrain the galaxy peculiar velocity distribution $f(w)$ (eg. Bean *et al.* 1983, Davis and Peebles 1983). The redshift space correlation function $\xi(\sigma, \pi)$ is given by convolving the real space

correlation function $\xi(r)$ with $f(w)$,

$$1+\xi(\sigma,\pi)=\int_{-\infty}^{\infty}[1+\xi(r)]f[w_3+H_0\xi(1+\xi)^{-1}r_3]dw_3, \tag{8}$$

(Bean *et al.* 1983), where $r^2=\sigma^2+r_3^2$, $r_3=\pi-w_3/H_0$ (the subscript 3 denotes the line-of-sight component of a vector quantity) and $\langle w\rangle=-H_0\xi(1+\xi)^{-1}r$ is the mean streaming velocity in an $\Omega=1$ Universe.

We have measured $\xi(\sigma,\pi)$ in four σ bins each of width $2h^{-1}$Mpc centred on 1, 3, 5 and $7h^{-1}$Mpc — Figures 3*a* and *b* for the data and simulations respectively. We have calculated the best-fit rms peculiar velocity, $\langle w^2\rangle^{1/2}$, for three models for $f(w)$, a Gaussian,

$$f(w)=\frac{1}{\sqrt{2\pi}\langle w^2\rangle^{1/2}}\exp\left(\frac{-w^2}{2\langle w^2\rangle}\right), \tag{9}$$

a $|w|^{3/2}$ distribution,

$$f(w)=\frac{0.476}{\langle w^2\rangle^{1/2}}\exp\left(\frac{-0.7966|w|^{3/2}}{\langle w^2\rangle^{3/4}}\right), \tag{10}$$

and an exponential distribution,

$$f(w)=\frac{1}{\sqrt{2}\langle w^2\rangle^{1/2}}\exp\left(\frac{-\sqrt{2}|w|}{\langle w^2\rangle^{1/2}}\right). \tag{11}$$

The optimum value of $\langle w^2\rangle^{1/2}$ for each distribution was calculated by maximizing the likelihood

$$\mathcal{L}=\prod_{\pi-\mathrm{bins}}[2\pi\mathrm{Var}\{\xi(\sigma,\pi)\}]^{-1/2}\exp\left[\frac{-(\xi^o(\sigma,\pi)-\xi^p(\sigma,\pi))^2}{2\mathrm{Var}\{\xi(\sigma,\pi)\}}\right], \tag{12}$$

where $\xi^o(\sigma,\pi)$ is the observed redshift space correlation function, $\mathrm{Var}\{\xi(\sigma,\pi)\}$ is the observed variance in $\xi^o(\sigma,\pi)$ from bootstrap resampling and $\xi^p(\sigma,\pi)$ is the predicted correlation function from (8). The continuous, dashed and dot-dashed lines in Figure 3 are the best fit curves for the Gaussian, $|w|^{3/2}$ and exponential models respectively. The best-fit values of $\langle w^2\rangle^{1/2}$ together with 95% confidence limits as estimated from likelihood ratios are given in Table 1.

For the survey data, we see that the exponential velocity distribution model gives a slightly better fit to the observations than the $|w|^{2/3}$ or Gaussian distributions. There is no obvious trend of $\langle w^2\rangle^{1/2}$ with separation σ, the 95% confidence range for $\langle w^2\rangle^{1/2}$ is roughly 200–1100 km s^{-1}, with a maximum likelihood value around 500 km s^{-1}. Note that our survey does not provide a strong constraint on small scale peculiar velocities simply due to the sparse-sampling strategy we have employed. It would be interesting to compare $f(w)$ for the morphological and luminosity-selected subsamples defined in Paper 2, but unfortunately, the errors on $\xi(\sigma,\pi)$ for these subsamples are too large to test for variation of $\langle w^2\rangle^{1/2}$ with galaxy type or luminosity.

For the simulations, there is little to choose between velocity distribution models. There is a slight trend of decreasing $\langle w^2\rangle^{1/2}$ with separation σ, but the rms peculiar velocities remain larger than for the survey data on all scales. The simulations will therefore tend to slightly overestimate non-linearity in galaxy clustering on scales up to $8h^{-1}$Mpc.

3 Testing Estimators for β

In the preceding section we showed that the simulations have comparable two-point clustering statistics to the survey data and that small-scale peculiar velocities are slightly larger in the simulations than in the data. Therefore we can conservatively say that if the simulations obey linear theory on a certain scale then linear theory should also be applicable to the survey data on that same scale. In this section we investigate the scales on which linear theory is obeyed by the simulations.

3.1 Anisotropy of $\xi(\sigma, \pi)$

The redshift space spherical harmonics $\xi_l(r)$ in equation (4) are given by an integral over the full redshift space correlation function $\xi(r, \mu)$,

$$\xi_l(r) = \frac{2l+1}{2} \int_{-1}^{1} \xi(r, \mu) P_l(\mu) d\mu, \tag{13}$$

where $P_l(\mu)$ is the lth order Legendre polynomial. We can measure $\xi(r, \mu)$ by comparing the observed, weighted sum of galaxy pairs $w_{dd}(r, \mu)$ at separation r and direction cosine to line of sight μ, with the expected background $\mathrm{bgr}(r, \mu)$ for an isotropic, unclustered distribution. The line of sight direction is defined as the bisector in angle of each pair.

Since $P_l(\mu)$ is an odd function for odd l and an even function for even l, the odd-l harmonics vanish and the even-l harmonics are given by

$$\begin{aligned} \xi_l(r) &= (2l+1) \int_0^1 \left(\frac{w_{gg}(r, \mu)}{\mathrm{bgr}(r, \mu)} - 1 \right) P_l(\mu) d\mu \\ &\approx (2l+1) \Delta\mu \left[\sum_{\mathrm{pairs(r)}} \frac{w_i w_j P_l(\mu)}{\mathrm{bgr}(r, \mu)} \right] - \delta_{l0}. \end{aligned} \tag{14}$$

Here we have replaced the integral over $\xi(r, \mu)$ with respect to μ by the weighted and appropriately normalised sum of $P_l(\mu)$ for all galaxy pairs at separation r. The $w_i w_j$ are the products of the weights of each galaxy in the pair, given by equation (1) of Paper 2 and δ_{l0} is the Kronecker delta symbol, equal to unity for $l = 0$, zero otherwise. The background $\mathrm{bgr}(r, \mu)$ is obtained by linear interpolation in μ from a pre-calculated look-up table. We do not interpolate between r-bins, since the $\xi_l(r)$ are calculated in the same separation bins in which $\mathrm{bgr}(r, \mu)$ is tabulated. This look-up table is generated in ten fixed steps in $\Delta \log r$ and $\Delta\mu$ using a large catalogue of random points with the same selection function and within the same boundaries as the data, and using the same weighting scheme,

$$\mathrm{bgr}(r, \mu) = \frac{[w_{gr}(r, \mu)]^2}{w_{rr}(r, \mu)}. \tag{15}$$

Here $w_{gr}(r, \mu)$ and $w_{rr}(r, \mu)$ are the summed weights of galaxy-random and random-random pairs respectively. This definition of the background does not require one to estimate the mean density of the data and random catalogues to normalize ξ; instead the normalisation is determined using only those galaxies at separation r and cosine direction μ. Such an estimator gives more stable estimates of ξ on large scales than traditional estimators (Hamilton 1993b; Paper 2).

In Figure 4 we plot the $\xi_l(r)$ measured from the simulations as the points with error bars. Also shown by the curves are the linear-theory predictions for the $\xi_l(r)$ for a biased, low-density CDM

model ($\Gamma = 0.2$, $b = 1.10$, $\beta = 0.35$). In this theory, $\Gamma = \Omega_0 h$ determines the shape of the real-space correlation function, and β determines the redshift-space distortions. The value of the bias factor b was chosen to match the estimated value of bias in the simulations (§2.2).

We use the power spectrum of Efstathiou, Bond and White (1992) and equations (6)–(9) of Hamilton (1992) to calculate these linear-theory predictions. We see that the direction-averaged correlation function ξ_0 measured from the simulations agrees well with linear theory on scales as small as $2h^{-1}$Mpc. Non-linearity is a far more severe problem for the quadrupole (ξ_2) and hexadecapole (ξ_4) harmonics. The quadrupole harmonic is expected to be negative in the linear regime (Hamilton 1992) and so we plot $-\xi_2$ in Figure 4. The measured ξ_2 is in fact positive on scales $r \lesssim 15h^{-1}$Mpc suggesting that the non-linear 'fingers of God' dominate ξ_2 on these scales. The amplitude of ξ_2 is lower than that predicted by linear theory until $r \approx 30h^{-1}$Mpc, suggesting that non-linearity may affect ξ_2 out to these scales. Beyond $\sim 55h^{-1}$Mpc the data is too noisy to measure ξ_2 reliably. The hexadecapole harmonic ξ_4 has an amplitude on scales $r \lesssim 15h^{-1}$Mpc exceeding the linear theory prediction by several orders of magnitude (in fact it is comparable to the direction-averaged correlation ξ_0) and on larger scales, it's measurement is too noisy to be useful.

Equation (4) gives physically reasonable estimates of the quantity β over a range of scales 21–42 h^{-1}Mpc: $\beta = 0.06 \pm 0.43$, 0.47 ± 0.48 and 0.02 ± 0.35 respectively at separations of $r \approx 21$, 30 and 42 h^{-1}Mpc. Comparison with the linear theory prediction suggests that the first of these estimates (at $r \approx 21h^{-1}$Mpc) is probably biased low by non-linearity, but the second two estimates appear to be in the linear regime.

3.2 Ratio $\xi(s)/\xi(r)$

With an N-body simulation, one has the advantage of being able to estimate the real space correlation function directly by using the real space locations of the simulation galaxies in (6), as well as via inversion of the projected correlation function (7). The former estimate of $\xi(r)$ is useful for studying effects of non-linearity in the simulations, whereas the latter, noisier, estimate gives a more realistic assessment of what we can hope to measure from real data. We have used the ratio $\xi(s)/\xi(r)$ measured with both $\xi(r)$ estimates in equation (5) to estimate β on a range of scales. These estimates are presented in Figures 5a and b for the direct and projected estimates of $\xi(r)$ respectively.

In Figure 5a, we see that β appears to converge (assuming that b is independent of scale) by scales $r \approx 5h^{-1}$Mpc. Beyond $r \approx 20h^{-1}$Mpc, the measured correlation functions are too noisy to usefully constrain β. We have calculated the maximum-likelihood value of β from the simulations over the separation range 5–20 h^{-1}Mpc, and find $\beta = 0.56$. This is shown by the horizontal line in the figure. The dotted lines show the 95% confidence limits on β, the points at which the likelihood has fallen by a factor of 6.82 from its maximum value. This range is $0.19 < \beta < 0.94$.

In Figure 5b, we see that the estimates of β using the projected $\xi(r)$ estimate show, unsurprisingly, larger error bars. On scales 5–20 h^{-1}Mpc, the measured values of β are consistent with the 'direct' estimation of $\xi(r)$. Over these scales, the maximum-likelihood value of β is 0.59, with 95% confidence limits $0.04 < \beta < 1.13$.

Values of β estimated from the ratio $\xi(s)/\xi(r)$ are rather larger than the intrinsic $\beta \approx 0.35$ for the simulations. Part of the reason for this may be that scales $\sim 8h^{-1}$Mpc are mildly non-linear

(§3.3), and hence b_8 may be slightly biased with respect to $b_{\rm lin}$. Additionally, the error bars on the ratio $\xi(s)/\xi(r)$ are large and the 95% confidence limits certainly include $\beta = 0.35$. In the following subsection we use the ratio of the volume integrals, J_3, of the galaxy correlation function in order to obtain a less noisy estimate of β.

3.3 Ratio $J_3(s)/J_3(r)$

A less noisy estimator of galaxy clustering is the volume integral over the correlation function,

$$J_3(r) = \int_0^r x^2 \xi(x) dx. \tag{16}$$

We measure J_3 as follows. The contribution to J_3 on scales 0–$r_{\rm min}$, where $r_{\rm min}$ is the smallest scale at which $\xi(r)$ was measured, is calculated from extrapolation of a power-law fit to $\xi(r)$, $\xi(r) = (r/r_0)^{-\gamma}$,

$$J_3(r_{\rm min}) = \frac{r_0^\gamma}{3-\gamma} r_{\rm min}^{3-\gamma}. \tag{17}$$

This contributes to less than 1% of $J_3(8h^{-1}{\rm Mpc})$ for $r_{min} = 0.1h^{-1}{\rm Mpc}$, and so the validity of extrapolating a power-law to zero separation is not crucial. Contributions to J_3 from scales over which $\xi(r)$ has been measured are determined simply by multiplying the volume of each separation bin by the value of ξ measured in that bin,

$$J_3(r_k^{\rm hi}) = J_3(r_{\rm min}) + \frac{1}{3}\sum_{i=1}^{k} [(r_i^{\rm hi})^3 - (r_i^{\rm lo})^3]\xi_i. \tag{18}$$

Note that each measured ξ is already weighted towards the outer edge of each bin, simply due to the increasing number of total galaxy pairs with separation (assuming that the bins are narrow enough that $\xi(r)$ does not change significantly across the bin), and so nothing is gained by interpolating between bins. Note also that as each contribution to J_3 is added to the sum over bins, the current value of J_3, being an integral quantity, corresponds to the radius of the *outermost* edge of the last bin added.

In Figure 6, we plot β determined from the ratio $J_3(s)/J_3(r)$ from the simulations using $J_3(r)$ obtained by (a) integrating the direct estimate of $\xi(r)$ and (b) integrating the projected estimate of $\xi(r)$. We see that non-linearities affect the J_3 integral to slightly larger scales (about $15h^{-1}$Mpc) than ξ estimates. On a scale of $17.8h^{-1}$Mpc we find a value $\beta = 0.29 \pm 0.23$ from Fig. 6a and $\beta = 0.36 \pm 0.43$ from Fig. 6b. Although rather smaller than the estimates from $\xi(s)/\xi(r)$, these values are consistent given the size of the error bars.

3.4 Conclusions from Simulations

We have analysed an ensemble of CDM-like N-body simulations, which give a reasonable match to the real and redshift space correlation functions measured from the Stromlo-APM Redshift Survey and which have comparable, but slightly larger, peculiar velocities $\langle w^2 \rangle^{1/2}$. We find that the 2nd and 4th order spherical harmonics of the redshift space correlation function are severely affected by non-linearities to scales $r \sim 30h^{-1}$Mpc, and so one needs a reliable measurement of the ξ_l on

scales $r \gtrsim 30h^{-1}$Mpc in order for linear theory to be applicable. This is in agreement with the Fourier-space harmonic analysis of Cole *et al.* (1994).

On the other hand, the direction averaged correlation function ξ_0 is only weakly affected by non-linearity; non-linear effects become unimportant on much smaller scales, $r \sim 5h^{-1}$Mpc. Thus the more practical method for determining β from present-generation redshift surveys is by comparison of the direction-averaged redshift-space correlation function with the real-space correlation function. By using the J_3 volume integral over ξ, one decreases the random noise in β, at the expense of increasing the scale of non-linearity to $\sim 15h^{-1}$Mpc. In practice it will probably be worthwhile estimating β from both $\xi(s)/\xi(r)$ and $J_3(s)/J_3(r)$. We expect the J_3 ratio to give the less noisy results.

4 Results from Stromlo-APM Survey

4.1 Constraints on β

We have measured the spherical harmonics $\xi_l(s)$ of the Stromlo-APM redshift space correlation function in the same way as for the simulations (§3.1). The results are shown as the points with error bars in Figure 7. The curves show the same linear theory predictions as in Figure 4. We see pronounced effects of non-linearity and very large error bars on the ξ_2 and ξ_4 harmonics on scales smaller than $20h^{-1}$Mpc. The direction-averaged correlation function ξ_0 is well matched by the linear theory prediction on all scales. On scales of 21, 30 and 42 h^{-1}Mpc, the estimated values of β are 0.41 ± 0.17, -0.03 ± 0.29 and 0.23 ± 0.31 respectively.

We expect the ratios of the direction-averaged clustering in redshift space and real space to give more reliable estimates of β. In Figure 8*a*, we plot our estimates of β from the redshift survey, as determined from the ratio $\xi(s)/\xi(r)$. Although there is quite a wide scatter in the β estimates on different scales, there is no obvious systematic trend with separation, and so we have calculated the maximum-likelihood value of β using the three data points in the range 5–12 h^{-1}Mpc. We find $\beta = 0.36$ with 95% confidence limits -0.03–0.75. Using the $J_3(s)/J_3(r)$ ratio (Fig. 8*b*), we find a value of $\beta = 0.48 \pm 0.12$ at $r = 17.8h^{-1}$Mpc.

All three estimates of β give consistent results and all exclude the possibility of $\beta \gtrsim 0.75$ at very high confidence.

4.2 Disentangling Ω and b

Ideally, of course, one would like to know the values of the density parameter Ω and the bias parameter b individually. Cole *et al.* (1994) have discussed how it may be possible with future redshift surveys to separate the determination of Ω and b by studying the scaling of non-linear effects. An alternative approach is the study of high order correlations to constrain the (possibly non-linear) biasing model using weakly non-linear perturbation theory. Gaztañaga and Frieman (1994) have used high order moments of APM galaxies to constrain biasing models. To be consistent with non-linear perturbation theory, one should allow the possibility of *non-linear* bias, in which case second- and third-order non-linear bias coefficients can be chosen which match the observed

high order correlations. However, the observations are very well fit by an *unbiased*, low-density CDM model with $b \approx 1$. Applying Occam's razor, this seems the more natural solution.

4.3 Relative Biasing of Different Galaxy Types

Despite the uncertainties in the value of galaxy bias with respect to the mass, one may study the *relative* bias of galaxies of different type by comparing their clustering properties. There are two independent ways to measure the relative bias factors: (1) by comparing real-space clustering in the linear regime and (2) by measuring the redshift space amplification of clustering due to equation (5). One thus has a consistency check on measurements of β and relative bias parameters. We have already compared the clustering of galaxies of different luminosity and morphological type in Paper 2. In that paper we concentrated on the small-scale (power-law) regime of galaxy clustering. Here we study clustering in the linear regime. We analyse galaxy subsamples from the Stromlo-APM survey of low, middle and high luminosity, and of early and late type. These galaxy samples are defined in Table 1 of Paper 2.

In Figure 9 we plot the relative bias values $b_t = \xi_{tg}(r)/\xi_{gg}(r)$ for each sample over a range of scales. We have divided the real-space cross-correlation of each sample with the parent APM galaxy sample (Paper 2) by the real-space cross-correlation function of the 'all galaxies' sample, hence the relative bias for the 'all galaxies' sample is defined to be unity. The error bars are determined from the one sigma scatter in b_t from the nine bootstrap-resampled versions of the survey data. Given that our estimates of $\xi(r)$ are unreliable beyond $r \approx 20h^{-1}$Mpc, we see no obvious trend of relative bias with scale in the linear regime. We have therefore calculated the maximum-likelihood value of b_t over the range 5–12 h^{-1}Mpc. These values, along with the 95% confidence limits, are given in Table 2. We see that low-luminosity galaxies (sample b), are only about one third as strongly clustered as middle-luminosity galaxies, in accordance with the findings of Paper 2. High luminosity galaxies (sample d) appear to be about thirty percent more strongly clustered than middle-luminosity galaxies, although the 95% confidence limits do allow for no difference in clustering, again in accord with Paper 2. Early type galaxies (e) have a very similar bias parameter to luminous galaxies, whereas late type galaxies have a bias parameter midway between that of low and middle-luminosity galaxies.

Figure 10 shows the relative bias values determined from the ratio $J_3^{tg}(r)/J_3^{gg}(r)$. These results show smaller scatter than the $\xi_{tg}(r)/\xi_{gg}(r)$ ratios and give consistent results in the linear regime. The relative bias measured at a separation of $r = 17.8h^{-1}$Mpc is shown in Table 2.

The parameter most commonly used for normalizing clustering models and theories to observations is the variance of galaxy counts in $8h^{-1}$Mpc radius spheres, $(\sigma_8^2)_g$,

$$(\sigma_8^2)_g = \frac{1}{V^2} \int \int_V \xi(r_{12}) dV_1 dV_2. \tag{19}$$

We estimate $(\sigma_8^2)_g$ by Monte-Carlo integration of the observed real-space correlation function for each of the galaxy samples using 500,000 randomly chosen pairs of points inside an $8h^{-1}$Mpc radius sphere. Results are given in Table 2. As we see from Figure 6, $(\sigma_8^2)_g$ may be mildly affected by non-linearity, and so we do not expect b_t and $(\sigma_8)_g$ to be directly proportional. Note the significant difference in $(\sigma_8^2)_g$ for galaxies fainter than L^* and those around L^* and brighter.

In Figure 11 we plot estimates of β for each galaxy sample. In order to estimate β for galaxy subsamples, we have measured the redshift-space cross-correlation function of the given galaxy sample

with the all-galaxies sample using the estimator

$$1 + \xi_{tg}(s) = \frac{w_{tg}(s) w_{rr}(s)}{w_{tr}(s) w_{gr}(s)}. \tag{20}$$

Here the subscript t denotes galaxies of specific type, g denotes all galaxies and r denotes random points (cf. eq. 6). Comparing this with the real-space cross correlation function $\xi_{tg}(r)$ gives an estimate of β via equation (5). Once again, the error bars come from the scatter between bootstrap resamplings. Estimates of β and 95% confidence limits over the separation range 5–12 h^{-1}Mpc are given in Table 2. Clearly, negative values or lower limits on β are not physically reasonable, but the upper limits are still useful. For instance, for bright galaxies (d) we can say that $\beta < 0.9$ with 95% confidence.

In Figure 12 we plot estimates of β using the ratio $J_3(s)/J_3(r)$ for each subsample. In Table 2, we give the value of β and its one sigma error at $r \approx 17.8 h^{-1}$Mpc

Now, if the 'true' bias factor $b_t^{\rm true}$ (ie. the bias with respect to the mass) is related to the relative bias factor by $b_t^{\rm true} = b_0 b_t$, (so that b_0 is the bias factor for the 'all galaxies' sample) then the product $b_t \beta$ for all galaxy samples should be a constant equal to $\Omega^{0.6}/b_0$. While we do find some scatter in this quantity between the different samples, the results are consistent ($\Omega^{0.6}/b_0 \approx 0.2$–$0.6$) within the 95% confidence limits.

5 Conclusions

We have used large and realistic N-body simulations to investigate the effects of non-linearity on two estimators for the quantity β (eqs. [4] and [5]). We find that non-linearity is important in the 2nd order spherical harmonic $\xi_2(s)$ of redshift space clustering to scales as large as $30h^{-1}$Mpc. In contrast, the direction-averaged correlation function $\xi_0(s)$ is only weakly affected by non-linearity on scales $r \gtrsim 5h^{-1}$Mpc. Therefore the most practical method for constraining β with existing redshift surveys is by measuring the amplification of direction-averaged redshift space clustering over real space clustering. An alternative approach, modeling the non-linearity, has recently been used by Cole *et al.* (1995).

Using the projected cross-correlation of Stromlo-APM galaxies with the parent APM galaxy survey enables a reliable determination of $\xi(r)$ on linear scales $r \gtrsim 5h^{-1}$Mpc. The ratio $\xi(s)/\xi(r)$ on scales 5–12 h^{-1}Mpc yields a value $\beta \approx 0.36$. The integral J_3 is less noisy than $\xi(r)$ and on a scale $r \approx 17.8h^{-1}$Mpc $J_3(s)/J_3(r)$ provides the estimate $\beta = 0.48 \pm 0.12$. Although a little lower than estimates of β from peculiar velocity analyses (eg. Hudson *et al.* 1995, who find $\beta = 0.74 \pm 0.13$), the large errors on *all* current estimates of β means they are all consistent. See Dekel (1994) or Strauss and Willick (1995) for a review of recent measurements of β.

The Stromlo-APM survey is a powerful sample for constraining β since the large volume probed enables us to reliably measure redshift space galaxy clustering in the linear regime, whereas many previous analyses have been limited to measuring $\xi(s)$ in the non-linear regime. Cross-correlation with the fully-sampled APM galaxy survey enables us to measure $\xi(r)$ much more accurately than using the angular correlation function $w(\theta)$, and thus the technique of using the ratio $\xi(s)/\xi(r)$ [or $J_3(s)/J_3(r)$] comes into its own for this survey.

With linear theory and 2-point clustering statistics alone one cannot separate the contributions of Ω and b to β. However, as Gaztañaga and Frieman (1994) have discussed, higher order correlations may be used to constrain biasing models. Their analysis of APM galaxies favours a linear bias parameter $b \approx 1$, although to be strictly self-consistent, one should allow for a non-linear bias model in non-linear perturbation theory, in which case one can always match the observed skewness of APM galaxy counts in cells by adjusting the non-linear bias parameters. Further work is clearly required in constraining possible biasing models.

As we have seen in Paper 2, different classes of galaxy have different clustering properties, and so not all galaxies can have exactly the same biasing parameter. In particular, low-luminosity galaxies are about three times less strongly clustered than L^* galaxies on large scales, and so $b_{L^*} \approx 3b_{<L^*}$. An interesting test would be to see if high order clustering of low-luminosity galaxies also predicts a lower value of bias than for L^* galaxies.

In conclusion, we find that a relatively low value of β is favoured by the Stromlo-APM data; we can certainly exclude an unbiased, $\Omega = 1$ model at more than 95% confidence. We thus conclude that $\Omega < 1$ and/or that galaxies are positively biased, ie. more strongly clustered than the underlying mass distribution.

Acknowledgments: we are indebted to Andrew Hamilton for invaluable e-mail correspondence and to Peter Quinn for useful discussions during the early stages of this project. We thank Albert Stebbins for pointing out an error in an earlier version of this paper.

Tables

Table 1: Constraints on galaxy peculiar velocities (km s^{-1}) for survey data and simulations.

Model	Gaussian				$\|w\|^{3/2}$				Exponential			
σ	$\langle w^2\rangle^{1/2}$	95% conf		$\ln(\mathcal{L})$	$\langle w^2\rangle^{1/2}$	95% conf		$\ln(\mathcal{L})$	$\langle w^2\rangle^{1/2}$	95% conf		$\ln(\mathcal{L})$
					SurveyData							
1.0	434	144	799	−10.6	442	158	867	−10.2	476	179	1156	−9.8
3.0	408	241	841	−4.3	468	260	925	−4.0	569	303	1106	−3.7
5.0	425	169	836	−3.0	446	179	896	−2.9	493	194	1063	−2.8
7.0	327	0	805	0.5	355	0	898	0.5	355	0	1140	0.5
					Simulations							
1.0	679	571	812	−6.3	727	592	870	−5.7	857	686	1084	−6.2
3.0	624	466	844	0.0	669	488	928	0.5	783	543	1146	0.8
5.0	474	355	628	6.8	505	372	685	6.6	586	415	832	5.9
7.0	497	338	709	6.1	531	359	772	6.1	615	403	930	6.0

Table 2: Relative bias b_ξ and b_{J_3}, variance in $8h^{-1}$Mpc cells $(\sigma_8^2)_g$, and redshift space distortion factors β_ξ and β_{J_3} for galaxy subsamples

	Type	b_ξ	95% conf		b_{J_3}	$(\sigma_8^2)_g$	β_ξ	95% conf		β_{J_3}
a	All	1.00	1.00	1.00	1.00 ± 0.00	0.90 ± 0.05	0.36	−0.03	0.75	0.48 ± 0.12
b	Faint	0.31	0.05	0.56	0.32 ± 0.18	0.40 ± 0.10	1.91	0.35	3.46	0.85 ± 0.71
c	Middle	1.05	0.85	1.26	1.15 ± 0.13	1.62 ± 0.16	0.26	−0.12	0.65	0.59 ± 0.29
d	Bright	1.34	0.78	1.89	1.45 ± 0.35	1.20 ± 0.15	−0.11	−1.14	0.91	0.19 ± 0.43
e	E&S0	1.39	0.83	1.95	1.36 ± 0.35	1.28 ± 0.25	0.44	−0.13	0.99	0.27 ± 0.59
f	Sp&Irr	0.78	0.62	0.95	0.87 ± 0.12	0.66 ± 0.05	0.30	−0.16	0.75	0.33 ± 0.45

REFERENCES

Bardeen, J.M., Bond, J.R., Kaiser, N. and Szalay, A.S., 1986, ApJ, 304, 15
Barrow, J.D., Bhavsar, S.P. and Sonoda, D.M., 1984, MNRAS, 210, 19p
Bean, A.J., Efstathiou, G., Ellis, R.S., Peterson, B.A. and Shanks, T., 1983, MNRAS, 205, 605
Cole, S., Fisher, K.B. and Weinberg, D.H., 1994, MNRAS, 267, 785
Cole, S., Fisher, K.B. and Weinberg, D.H., 1995, submitted to MNRAS
Croft, R.A.C. and Efstathiou, G., 1994, MNRAS, 267, 390
Davis, M. and Peebles, P.J.E., 1983, ApJ, 267, 465
Dekel, A., 1994, ARA&A, 32, 371
Efstathiou, G., Bond, J.R. and White, S.D.M., 1992, MNRAS, 258, 1p
Efstathiou, G., Ellis, R.S. and Peterson, B.A., 1988, MNRAS, 232, 431 (EEP)
Fisher, K.B., Davis, M., Strauss, M.A., Yahil, A. and Huchra, J.P., 1994a, MNRAS, 267, 927
Fisher, K.B., Scharf, C.A. and Lahav, O., 1994b, MNRAS, 266, 219
Gaztañaga, E. and Frieman, J.A., 1994, ApJ, 437, L13
Hamilton, A.J.S., 1992, ApJ, 385, L5
Hamilton, A.J.S., 1993a, ApJ, 406, L47
Hamilton, A.J.S., 1993b, ApJ, 417, 19
Heavens, A.F. and Taylor, A.N., 1994, submitted to MNRAS
Hudson, M., Dekel, A., Courteau, S., Faber, S.M. and Willick, J.A., 1995, MNRAS, in press
Kaiser, N., 1987, MNRAS, 227, 1
Loveday, J., Efstathiou, G., Peterson, B.A. and Maddox, S.J., 1992a, ApJ, 400, L43
Loveday, J., Peterson, B.A., Efstathiou, G. and Maddox, S.J., 1992b, ApJ, 390, 338 (Paper 1)
Loveday, J., Maddox, S.J., Efstathiou, G., and Peterson, B.A., 1995, ApJ, 442, 457 (Paper 2)
Maddox, S.J., Sutherland, W.J. Efstathiou, G., and Loveday, J., 1990a, MNRAS, 243, 692
Maddox, S.J., Efstathiou, G. and Sutherland, W.J., 1990b, MNRAS, 246, 433
Saunders, W., Rowan-Robinson, M. and Lawrence, A., 1992, MNRAS, 258, 134
Strauss, M.A. and Willick, J.A., 1995, submitted to Phys. Rep.
Tadros, H., Efstathiou, G., Loveday, J. and Peterson, B.A., 1995, in preparation
White, S.D.M., Davis, M. Efstathiou, G., and Frenk, C.S., 1987, Nature, 330, 351

Figure Captions

Figure 1 A contour plot of the full redshift space correlation function $\xi(\sigma,\pi)$ measured from the Stromlo-APM Redshift Survey as a function of separation parallel (π) and perpendicular (σ) to the line of sight and smoothed with a $\left\{\begin{array}{ccc} 1 & 2 & 1 \\ 2 & 4 & 2 \\ 1 & 2 & 1 \end{array}\right\}$ smoothing filter. The contours are plotted in fixed steps in $\log \xi$ from -3 to 1. Solid contours show values $\xi \geq 1$, dashed contours show values $\xi < 1$ (*i.e.* in the linear regime).

Figure 2 Comparison of the Stromlo-APM (solid symbols) and N-body (open symbols) correlation functions in (a) redshift space and (b) in real space.

Figure 3 (a) The redshift-space correlation function $\xi(\sigma,\pi)$ plotted as a function of separation π along the line of sight for four bins in projected separation σ. The points with error bars show $\xi(\sigma,\pi)$ calculated from the Stromlo-APM survey. The curves show predictions for three peculiar velocity distribution functions — see text for details. (b) As (a) but for an ensemble of CDM-like N-body simulations.

Figure 4 First three spherical harmonics for the redshift-space correlation function measured from N-body simulations (symbols) and predicted by $\Gamma = 0.2$, $\beta = 0.35$ linear CDM theory (curves). Filled circles and the continuous line shows the direction-averaged correlation function (ξ_0). Star symbols and the dashed line show the negative of the quadrupole harmonic ($-\xi_2$). Open circles and the dotted line show the hexadecapole harmonic (ξ_4).

Figure 5 Estimates of β as a function of separation from the N-body simulations using equation (5), (a) uses 'direct' estimation of $\xi(s)$ and $\xi(r)$, (b) uses the projected cross-correlation estimate of $\xi(r)$ (Eq. 7). The horizontal line shows the maximum-likelihood fit to β over the range indicated and the dotted lines show 95% confidence limits on β.

Figure 6 As Figure 5 but using the volume integrals J_3 in place of ξ.

Figure 7 First three spherical harmonics of the redshift-space correlation function measured from the Stromlo-APM survey. The linear theory curves are as in Figure 4.

Figure 8 (a) Estimates of β as a function of separation for the Stromlo-APM survey data using $\xi(s)$ and $\xi(r)$ in equation (5). The horizontal line shows the maximum-likelihood fit to β over the range indicated and the dotted lines show 95% confidence limits on β. (b) Same as (a), but using the volume integrals J_3 in place of ξ.

Figure 9 Relative bias factors for subsamples of the Stromlo-APM Survey, determined from the ratio $\xi_{tg}(r)/\xi_{gg}(r)$.

Figure 10 As Figure 9 but using the volume integrals J_3 in place of ξ.

Figure 11 Estimates of β for subsamples of the Stromlo-APM Survey, determined from the ratio $\xi_{tg}(s)/\xi_{tg}(r)$.

Figure 12 As Figure 11 but using the volume integrals J_3 in place of ξ.

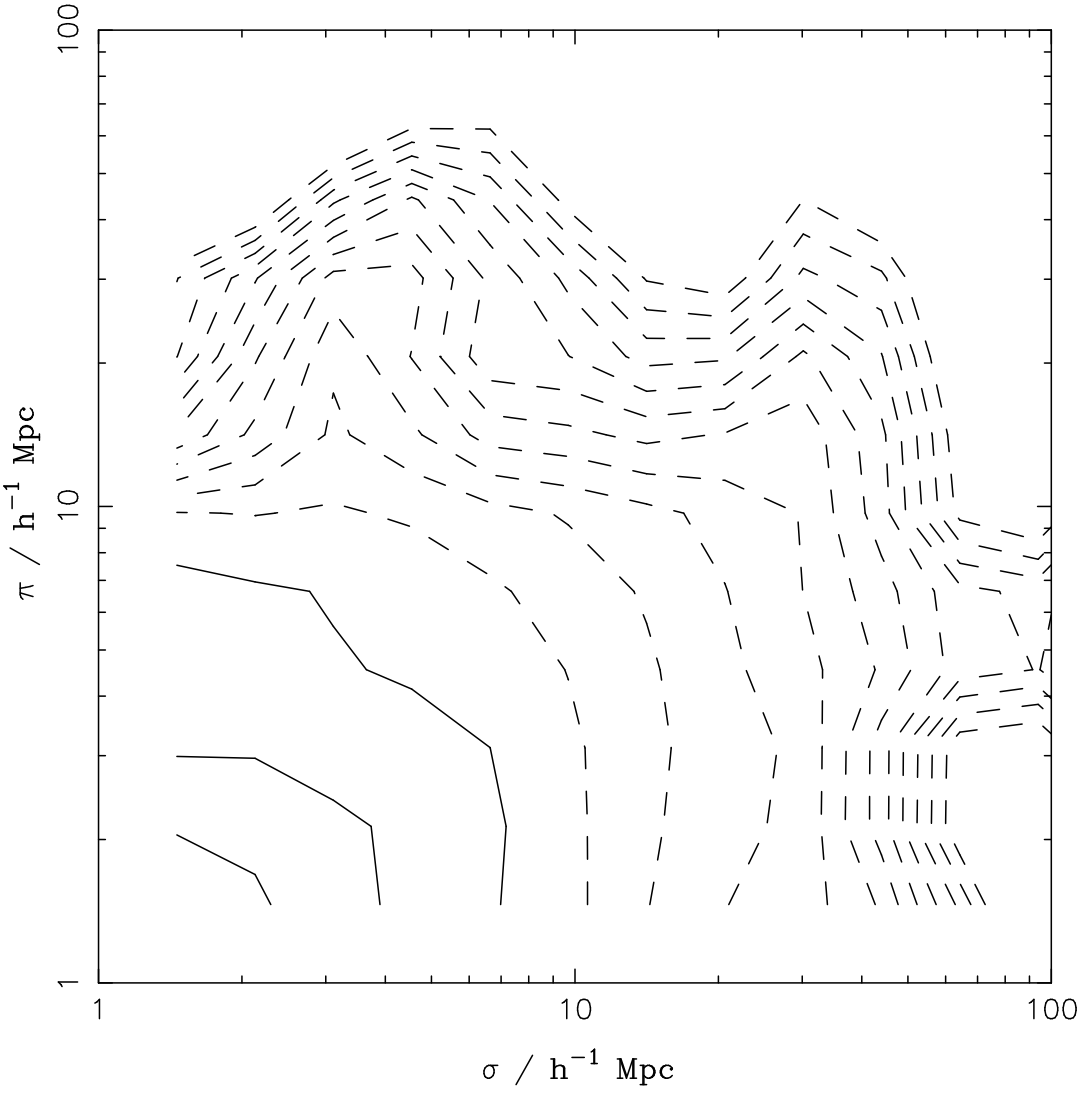

Figure 1:

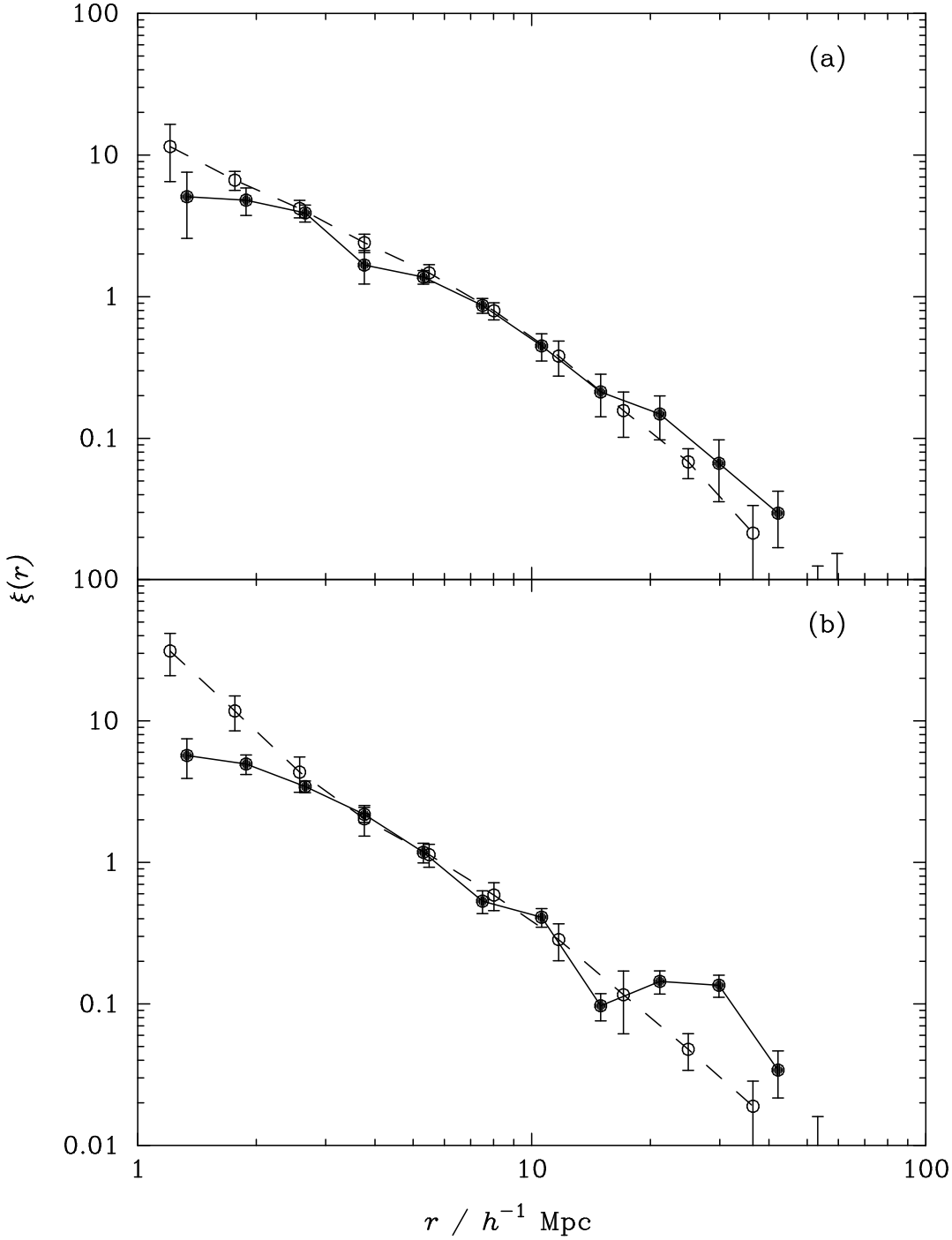

Figure 2:

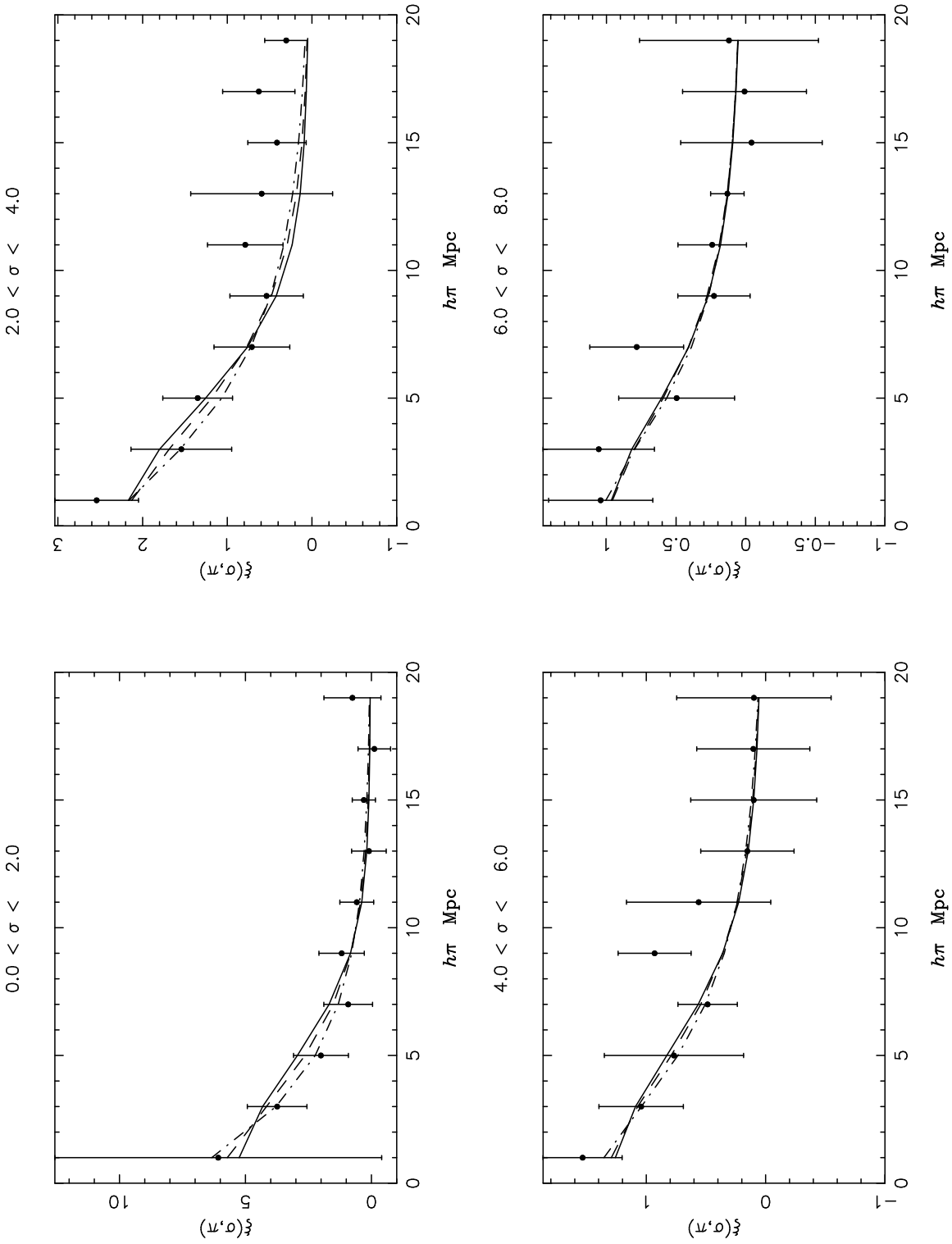

Figure 3: a

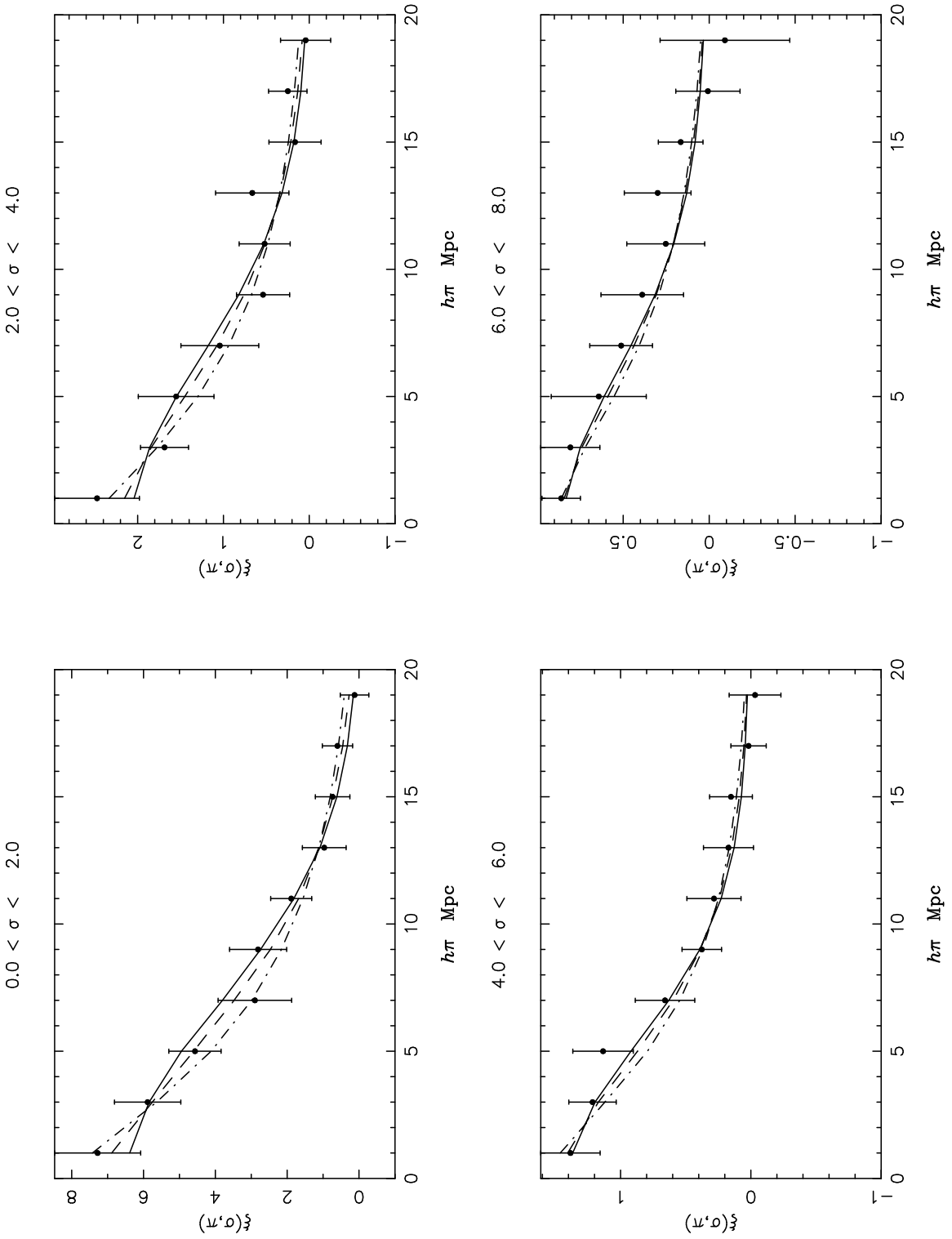

Figure 3: b

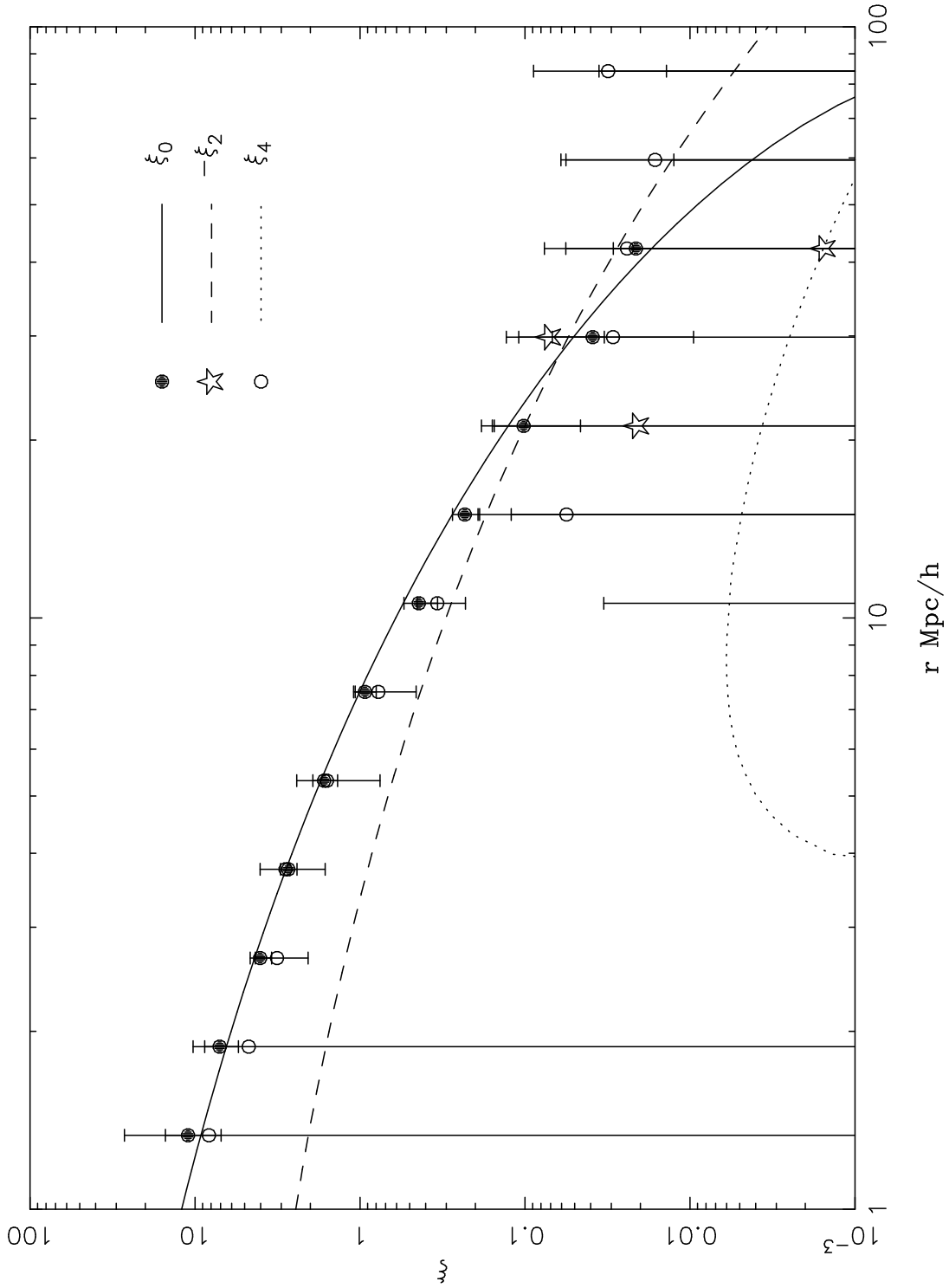

Figure 4:

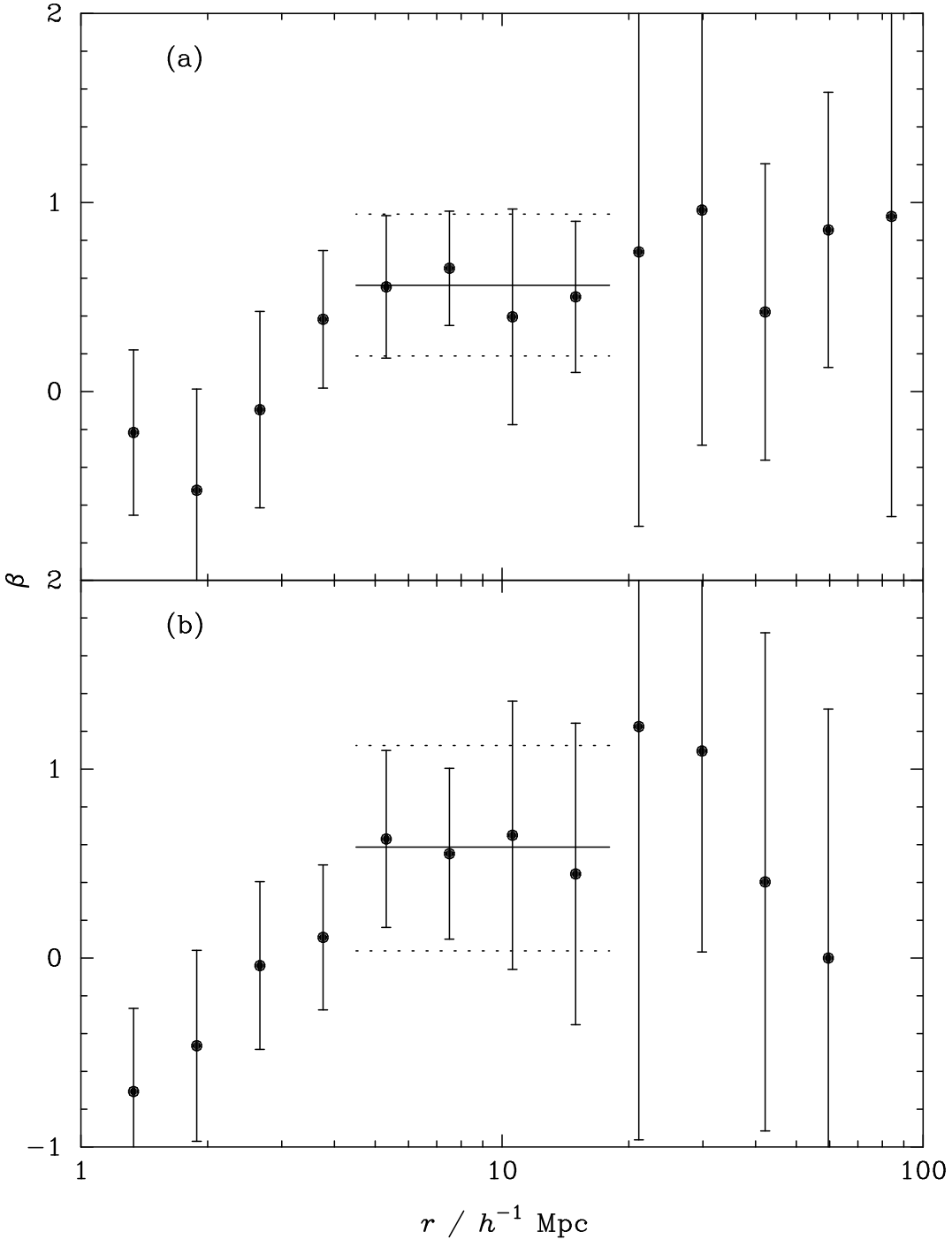

Figure 5:

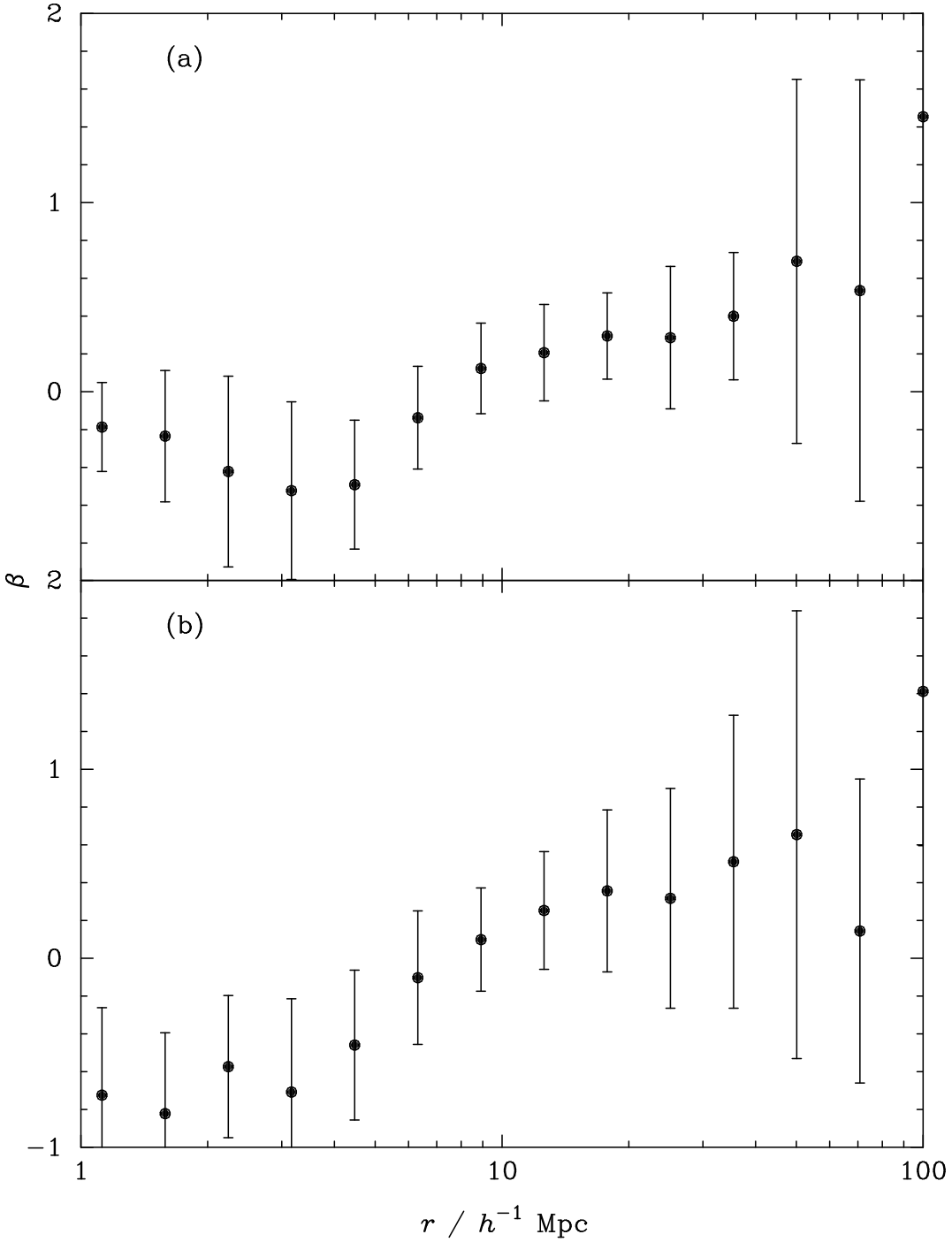

Figure 6:

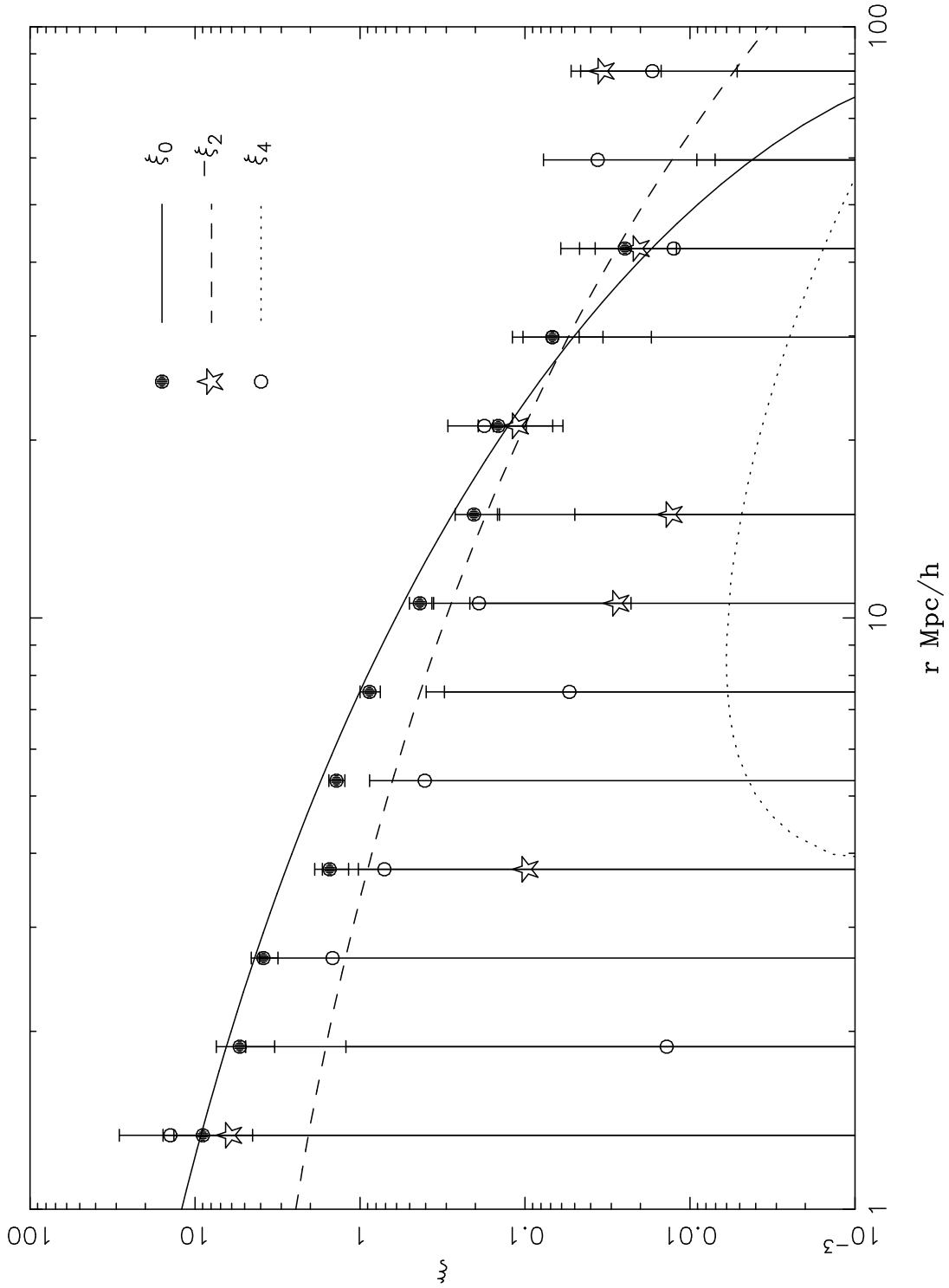

Figure 7:

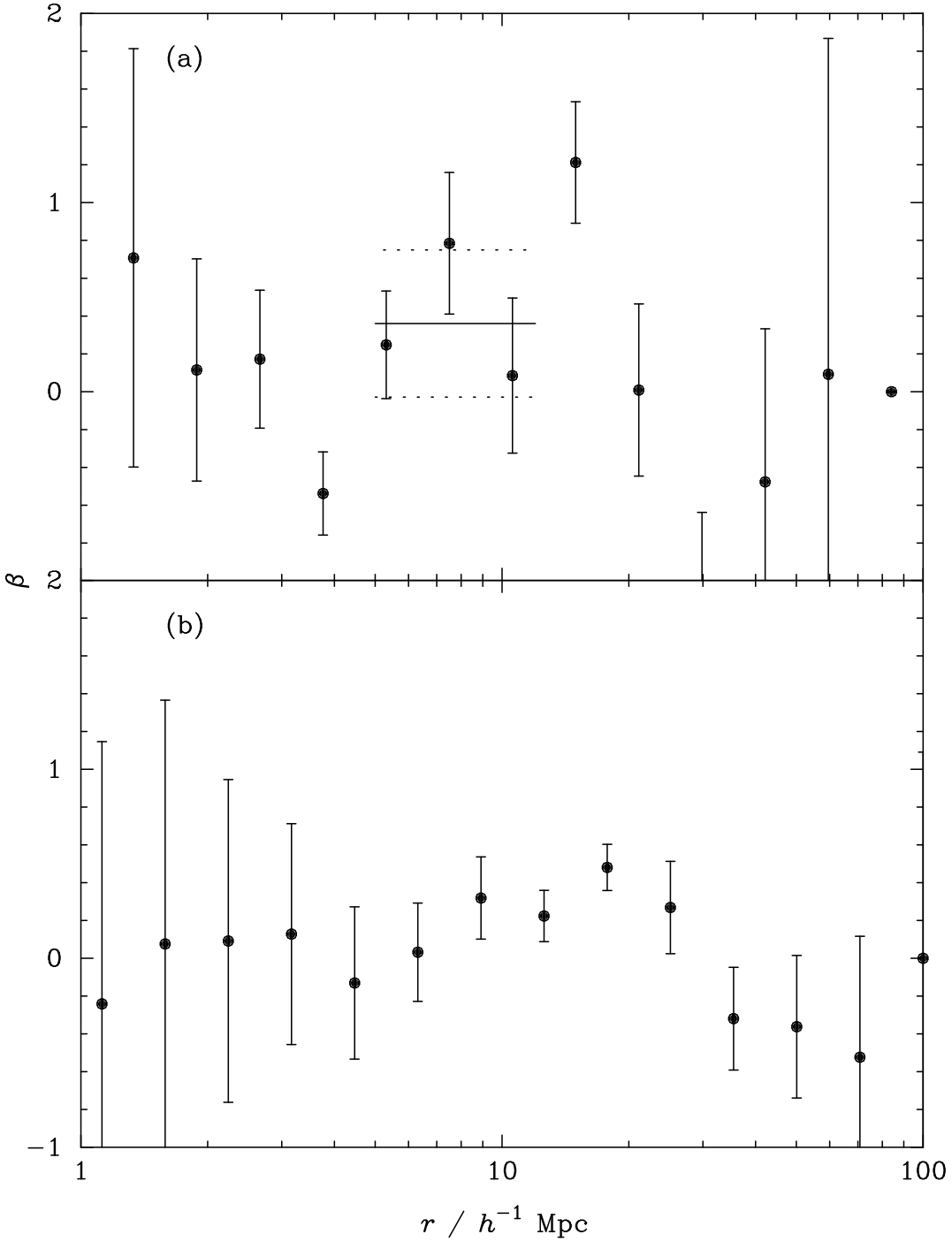

Figure 8:

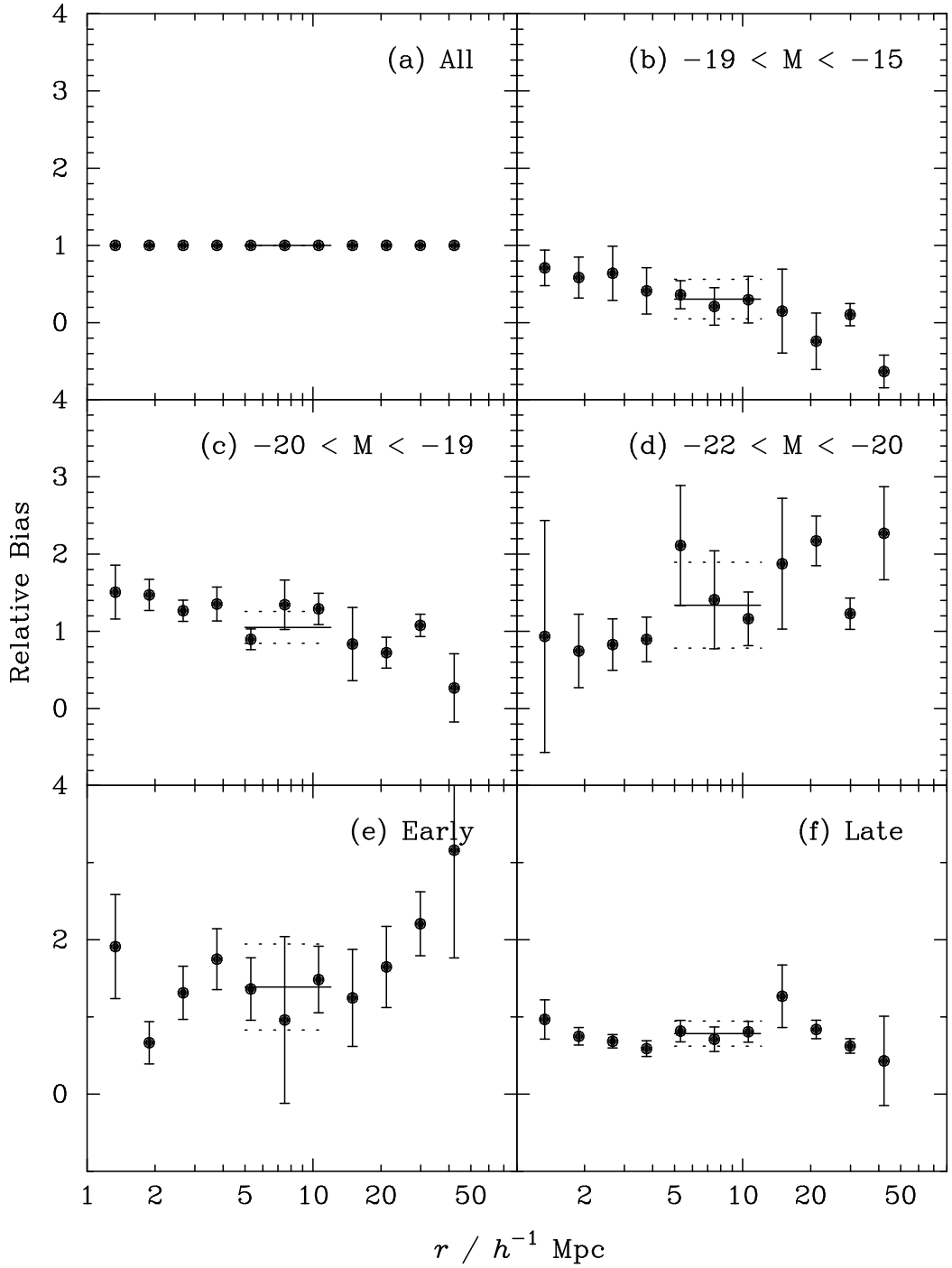
(a) All
(b) −19 < M < −15
(c) −20 < M < −19
(d) −22 < M < −20
(e) Early
(f) Late
Relative Bias
r / h^−1 Mpc

Figure 9:

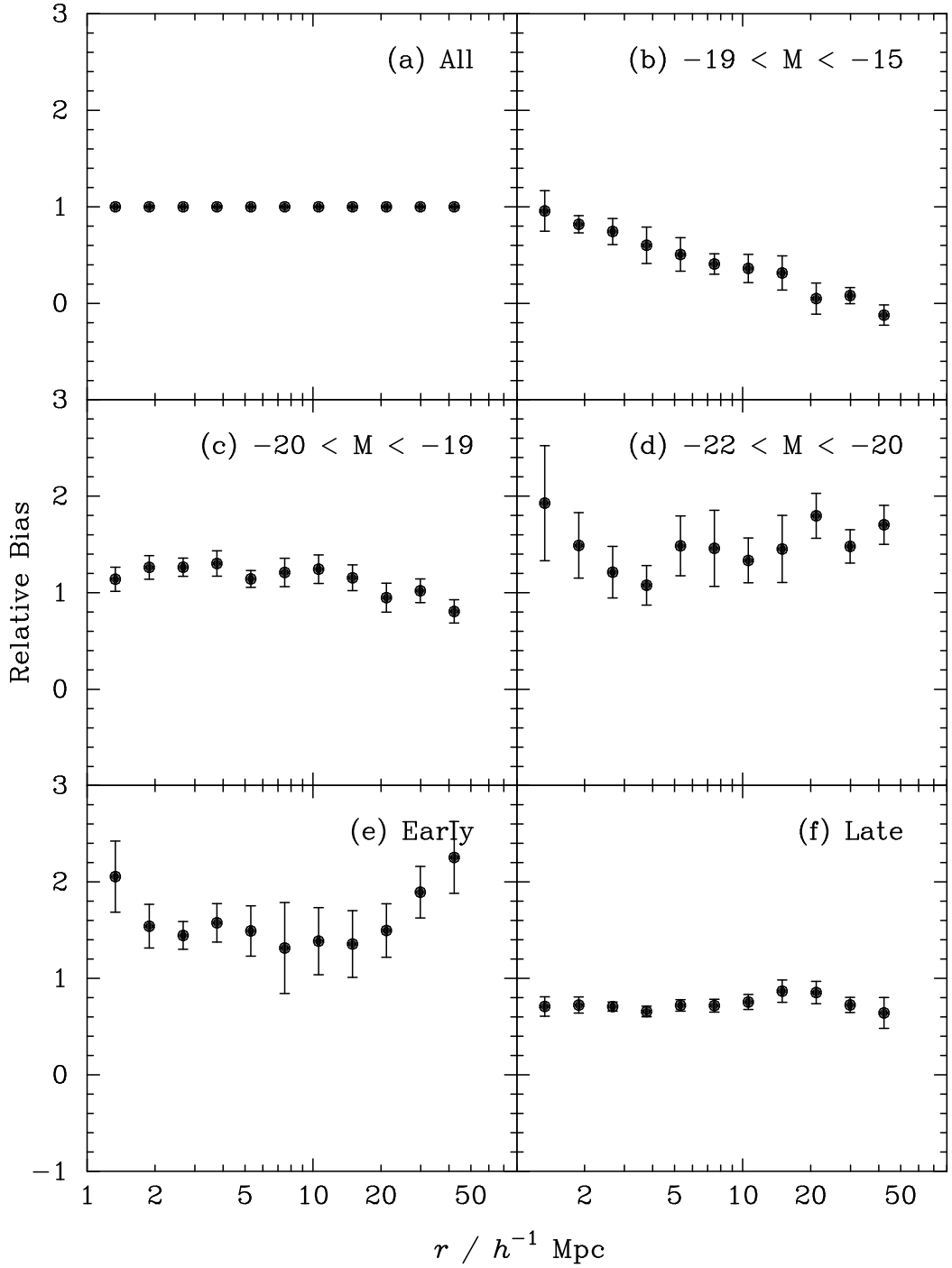
(a) All
(b) −19 < M < −15
(c) −20 < M < −19
(d) −22 < M < −20
(e) Early
(f) Late
Relative Bias
r / h^−1 Mpc
3
2
1
0
−1
1
2
5
10
20
50

Figure 10:

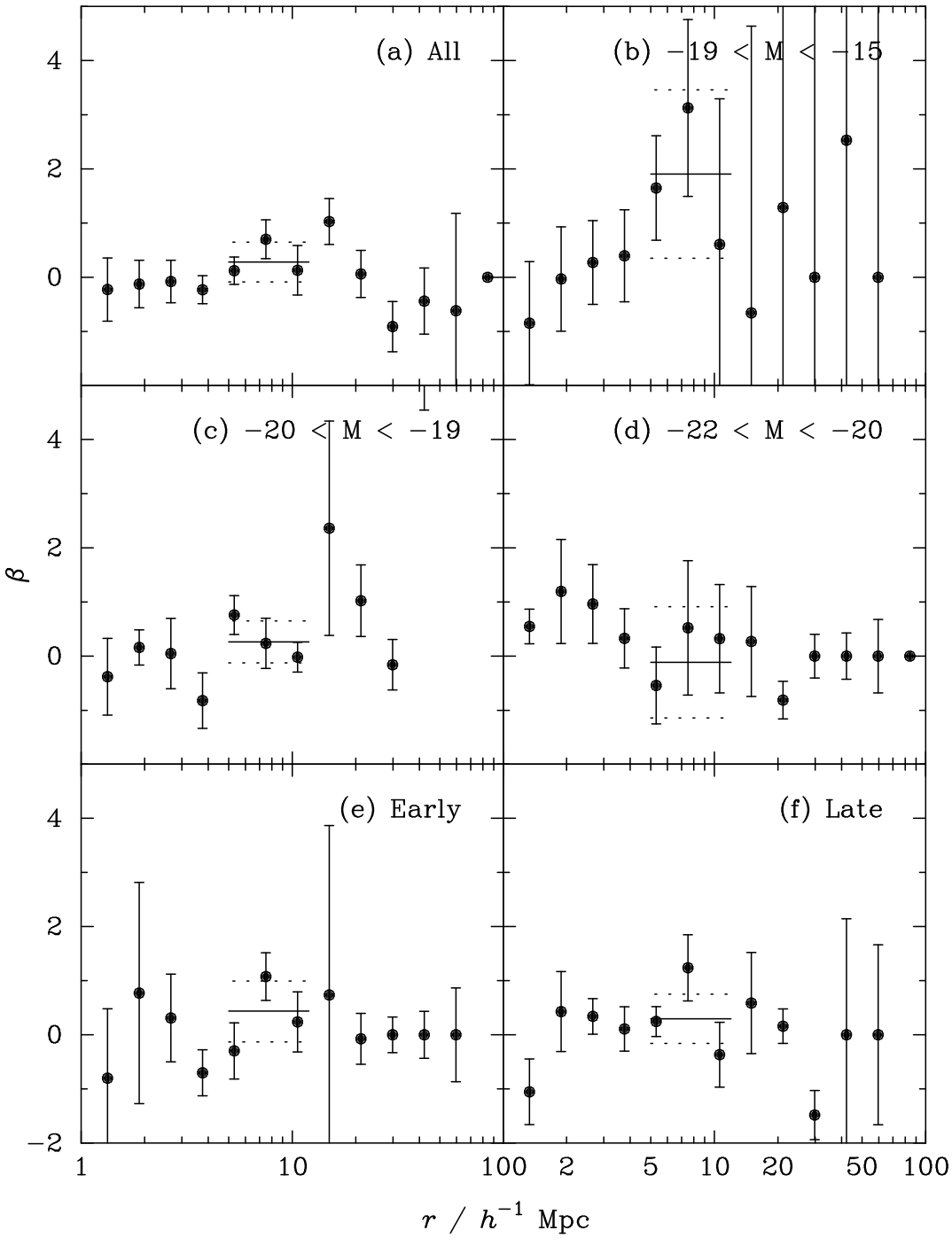

Figure 11:

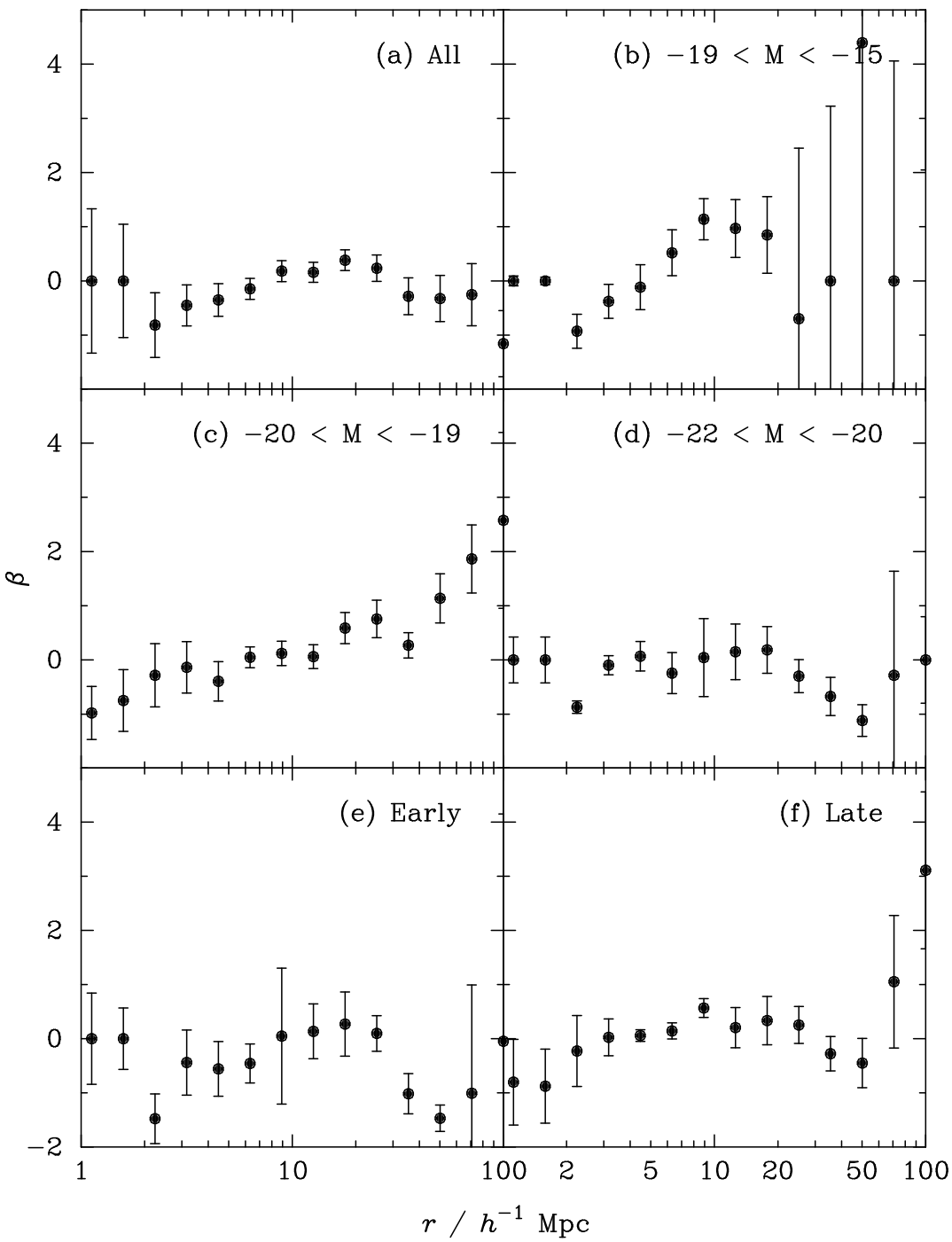
(a) All
(b) −19 < M < −15
(c) −20 < M < −19
(d) −22 < M < −20
(e) Early
(f) Late
β
4
2
0
−2
1
10
100
2
5
10
20
50
100
r / h^−1 Mpc

Figure 12: